Identification of ultrasound-contrast-agent dilution systems for ejection fraction measurements

Identification of Ultrasound Contrast Agent Dilution Systems for Ejection Fraction Measurements

Massimo Mischi, *Student Member, IEEE*, Annemieke H. M. Jansen, Antonius A. C. M. Kalker, *Fellow, IEEE*, and Hendrikus H. M. Korsten

***Abstract*—Left ventricular ejection fraction is an important cardiac-efficiency measure. Standard estimations are based on geometric analysis and modeling; they require time and experienced cardiologists. Alternative methods make use of indicator dilutions, but they are invasive due to the need for catheterization.**

This study presents a new minimally invasive indicator dilution technique for ejection fraction quantification. It is based on a peripheral injection of an ultrasound contrast agent bolus. Left atrium and left ventricle acoustic intensities are recorded versus time by transthoracic echocardiography. The measured curves are corrected for attenuation distortion and processed by an adaptive Wiener deconvolution algorithm for the estimation of the left ventricle impulse response, which is interpolated by a monocompartment exponential model for the ejection fraction assessment. This technique measures forward ejection fraction, which excludes regurgitant volumes.

The feasibility of the method was tested on a group of 20 patients with left ventricular ejection fractions going from 10% to 70%. The results are promising and show a 0.93 correlation coefficient with echographic bi-plane ejection fraction measurements. A more extensive validation as well as an investigation on the method applicability for valve insufficiency and right ventricular ejection fraction quantification will be an object of future study.

I. Introduction

The measurement of left ventricle (LV) ejection fraction (EF) is a common clinical practice. Usually the techniques for EF measurements are based on magnetic resonance imaging (MRI), ultrasound imaging, or nuclear imaging (positron emission tomography and single photon emission computed tomography) [1]–[8]. The acquired images are analyzed by manual or automatic segmentation. Once the end-diastolic (V_{ed}) and the end-systolic (V_{es}) volumes are estimated, the percent ejection fraction is defined as given in (1).

$$EF\% = \frac{V_{ed} - V_{es}}{V_{ed}} \cdot 100. \tag{1}$$

Manuscript received February 19, 2004; accepted August 21, 2004.

M. Mischi, A. A. C. M. Kalker, and H. H. M. Korsten are with the Technical University Eindhoven, The Netherlands (e-mail: m.mischi@tue.nl).

A. H. M. Jansen is with Catharina Hospital Eindhoven, The Netherlands.

H. H. M. Korsten is also with Catharina Hospital Eindhoven, The Netherlands.

A fast method for EF measurements, which is referred to as Teichholz technique [9], makes use of M-mode echocardiography and quantifies the EF based on the movement of the ventricular endocardium along one line [10]. More accurate estimates usually are derived from a LV bi-dimensional long-axis view, which provides information on a complete ventricular section [8], [11].

The use of a geometrical model is necessary to transform a bi-dimensional contour into a three-dimensional one (volume). A simple model assumes the ventricle to be represented by a stack of circles along the main axis (long axis) [5], [8]. If the information on a second ventricular section also is considered, the volume estimate can be derived from two perpendicular long axis planes (bi-plane method) [4], [5], [8]. This technique defines the ventricle as a stack of ellipses and adds one degree of freedom to the geometrical volume model. The result is an accurate interpolation of the ventricular endocardium [5]. However, none of these techniques, which are based on geometrical models, can detect abnormal shapes due to pathologic conditions (e.g., an aneurysm).

With MRI and advanced tri-dimensional ultrasound imaging, it is possible to measure the real contour for a series of short axes planes (normal to the long axis) [3], [6]. As tri-dimensional echocardiography is relatively new, MRI is well established and considered as the gold standard technique for EF and ventricular volume estimates [4], [11].

Unfortunately, geometric EF measurements are time consuming. The reliability of automatic border detection algorithms for echo images is sometimes very limited, and cardiologists prefer a manual delineation of the cardiac contours. As a consequence, the EF assessment procedure not only slows down the clinical practice dramatically but also requires the use of experienced cardiologists. Also MRI, despite the better image quality, requires a long procedure both for patient scanning and for data analysis, so that it does not suit emergency routines. Moreover, patients who are claustrophobic or have an implanted pacemaker cannot be scanned.

Geometric EF estimates do not consider blood volume transfers. Some patients present a significant insufficiency of the mitral valve. In this case, the geometric EF is the sum of two undistinguished terms: the forward EF (FEF), which is due to the blood volume that is ejected into the aorta, and the backward EF (BEF), which is due to the

blood volume that is ejected back into the left atrium (LA) due to mitral valve insufficiency. Only the FEF is a real indicator of the cardiac efficiency and is related to stroke volume and cardiac output.

The FEF assessment can be performed by use of indicator dilution techniques [12], [13]. A cold saline (thermodilution) or a dye (dye dilution) bolus is injected for the measurement [12], [13]. The injected indicator bolus is detected either in the LV or in the aorta out-track. The measurement is based on the detected indicator concentration and, therefore, is related to blood volume transfers. A mathematical interpretation of the measured indicator dilution curve (IDC, indicator concentration-versus-time curve) allows assessing the FEF [12].

A correct FEF estimation requires the bolus to be injected into the LV during diastole (Holt method [14]). In fact, the measurement must be performed in the LV (or aorta out-track) during contrast wash-out with no incoming contrast. Therefore, catheterization is needed, and the clinical application of the method is very limited due to the high invasiveness.

An invasiveness reduction is accomplished by use of radio-opaque contrast or radionuclides for X-rays or nuclear angiography. Videodensitometry of cine-loops can lead to FEF assessments [15], [16]. However, despite a noninvasive contrast detection, the contrast injection still needs cardiac catheterization (invasiveness issue), and the use of X-rays or radionuclides is not recommended in several situations.

The use of ultrasound contrast agents (UCA) opens new possibilities for minimally invasive indicator dilution measurements [17]–[27]. The UCA are microbubbles (diameter approximately from 1 to 10 μm [28], [29]) of gas stabilized by a shell of biocompatible material and are easily detectable by ultrasound investigation [30]–[33].

An UCA bolus is injected and detected by an ultrasound transducer in a specific site. In fact, due to its echogenecity, the diluted contrast produces an increase of backscattered acoustic intensity. The acoustic backscatter is related to the contrast concentration and can be used to generate IDCs. The UCA IDCs usually are interpreted by means of indicator dilution models, such as gamma variate, lognormal, compartmental, or random walk models, which are directly fitted to the curves [18], [19], [21], [34], [35].

In this study, UCA IDCs are not fitted and interpreted directly by a model. Instead, they are processed to characterize the dilution system between different IDC detection sites. In fact, the contrast dilution system between two contrast detection sites may be considered as a linear system and, therefore, characterized by its impulse response.

Unfortunately, even though the contrast dilution system is linear, the same is not true for the acoustic detection system. The measured acoustic intensity curve is distorted by nonlinearities that are introduced by both the ultrasound scanner and the contrast attenuation [26], [32], [36]. However, in the low contrast concentration range, the nonlinearities due to the ultrasound scanner signal processing are neglectable, and the attenuation effect can be modeled and compensated to generate a complete linear system [22], [33]. Once the complete system (UCA dilution and detection) is linear, the linear-system theory can be applied to obtain further information on the dilution process.

Outcome of the linear-system identification approach is a new method for the analysis of UCA dilution curves. A small dose of contrast is peripherally injected (typically in an arm vein) as a bolus and detected by a transthoracic ultrasound transducer. Acoustic intensity curves are measured by analysis of the B-mode output of the ultrasound scanner [37]. The scanner is set in power modulation mode in order to enhance the signal due to contrast acoustic backscatter [38]. The measured intensity curves are compensated for attenuation and transformed into real IDCs, which are linearly related to the contrast concentration.

Several IDCs are measured in different sites in the central circulation. A Wiener deconvolution technique is implemented to estimate the impulse response between the selected sites [39]–[42]. The choice for a least square error deconvolution algorithm is due to the small signal-to-noise ratio (SNR) of UCA acoustic intensity dilution curves. Specific models are then adopted to analyze the estimated impulse response.

In general, many clinical parameters can be assessed by estimation of impulse responses between different sites; however, in this study we focus on the FEF measurement. Two IDCs are measured in the LA and the LV. A Wiener deconvolution filter is applied to obtain the impulse response of the dilution system between LA and LV, i.e., the LV impulse response. The estimated impulse response corresponds to the LV IDC after a theoretical rapid injection of the contrast right into the LV. Therefore, the dilution system identification approach allows a minimally invasive FEF measurement without catheterization. Only a peripheral contrast bolus injection is needed.

The Wiener filter behavior is tested by specific simulation for different SNR and FEF. The FEF measurements then are validated in vivo. Twenty patients with EF going from 10% to 70% and no significant mitral insufficiency ($EF \simeq FEF$) were selected for the measurement. The EF was assessed by echographic bi-plane method applied to two- and four-chamber views with contrast opacification. The EF and FEF estimates were compared. The results show a 0.93 correlation coefficient between the two measurements.

II. Methodology

A. Ejection Fraction Measurement

The ejection fraction can be assessed by the measurement of the concentration of a diluted indicator [12], [24]. A ventricle can be modeled as a monocompartment system, whose volume changes as a periodic function of time. This can be represented by a cylinder-piston system as shown in Fig. 1. The system is filled with a fluid. Two

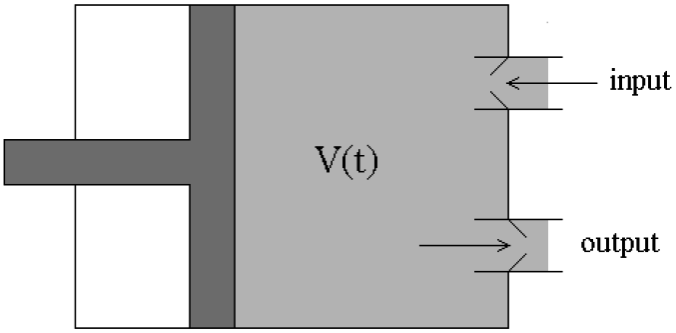

Fig. 1. Monocompartment, cylinder-piston model for LV simulation. An input and an output valve are included and represent the mitral and aortic valve, respectively.

valves are used for the fluid input and output and are driven by pressure changes. During diastole, the volume increases, the output valve is closed, and the input valve is open for the ventricle filling. During systole, the volume decreases, the input valve is closed, and the output valve is open for the ejection of the ventricular fluid.

If a contrast bolus is rapidly injected within a diastolic phase and the mixing is perfect, the contrast concentration at the end-diastolic phase is given by C_i and equals the injected indicator mass M divided by V_{ed}. During the following systole, part of the contrast mass (ΔM) in ejected out of the cylinder. The concentration C_{i+1} at the subsequent end diastole is given in (2).

$$C_{i+1} = \frac{M - \Delta M}{V_{ed}} = C_i \cdot \left(1 - \frac{V_{ed} - V_{es}}{V_{ed}}\right). \quad (2)$$

Combining (1) and (2), the percent EF can be expressed in terms of C_i and C_{i+1} as given in (3).

$$EF\% = \left(1 - \frac{C_{i+1}}{C_i}\right) \cdot 100. \quad (3)$$

The EF estimate in (3) only considers the fluid that is ejected through the output valve (aortic valve in the LV). If the input valve is insufficient (i.e., it leaks), part of the contrast is ejected back through the input valve (mitral valve in the LV). However, this fraction of contrast comes again into the ventricle during the subsequent diastole and, therefore, does not contribute to ΔM. As a consequence, the EF definition in (3) is better referred to as FEF.

Usually the SNR of measured IDCs is very low (SNR $= 20\log(A_{\max}/N) \simeq 15$ dB, where $A_{\max}$ and N are the IDC maximum amplitude and the noise amplitude respectively [18], [19]) and the definition of the right samples to estimate C_i and C_{i+1} is critical. A better approach is the use of an IDC model interpolation. The LV is well approximated by a simple monocompartment model, whose impulse response equals an exponential function (see Appendix). If C_0 is the concentration after a sudden indicator injection in the compartment at time $t = 0$, the IDC $C(t)$ is represented as given in (4), where τ is the time constant.

$$C(t) = C_0 \cdot e^{\frac{-t}{\tau}}. \quad (4)$$

The exponential function in (4) can be used to fit the IDC as measured from the model that is shown in Fig. 1. The ripple due to the pulsatile flow does not represent a problem because it is averaged over a large number of cycles. Once the exponential model is fitted to the IDC down-slope, the FEF is measured by (3) as given in (5), where Δt is the cardiac period.

$$FEF = 1 - \frac{C_{i+1}}{C_i} = 1 - \frac{e^{\frac{-(t+\Delta t)}{\tau}}}{e^{\frac{-t}{\tau}}} = 1 - e^{\frac{-\Delta t}{\tau}}. \quad (5)$$

Eq. (5) is commonly used for IDC FEF measurements. However, it is valid only when the contrast bolus is rapidly injected into the ventricle within a diastolic phase, which is the reason why indicator dilution techniques for FEF measurements require catheterization and ventricular injection [12].

Eq. (4) represents the LV contrast concentration curve after the ventricle is suddenly filled with concentration C_0. Therefore, (4) also can be interpreted as the impulse response of the LV. In fact, assuming a perfect mixing in the LV, the rapid contrast injection can be represented by a concentration impulse (expressed as a time-space Dirac function) passing through the mitral valve. As a result, the consequent LV concentration that is given in (4) expresses the LV impulse response function.

When the input function is not an impulse, a derivation of the impulse response of the ventricle still is possible. In fact, if the input and output concentration curves of the LV system are known, a deconvolution technique can be applied to identify the system and estimate its impulse response (see Section II-C). With the assumption of LA perfect mixing, the LA IDC represents the LV input function. As a result, the measurement of the LA and LV IDCs is sufficient for the LV system identification. The estimated impulse response satisfies the assumptions of (3), and (5) can be applied without further restrictions.

The advantage of using a system identification approach for FEF measurements consists of a substantial reduction of the invasiveness level. Ventricular injection and catheterization can be avoided, and the LV impulse response, represented by (4), can be derived from the LA and LV IDCs after a peripheral contrast bolus injection.

B. Ultrasound Contrast Agent Dilution Curves

The combined use of ultrasound and UCAs is a solution that allows the simultaneous measurement of several IDCs from different sites in the central circulation. In fact, several regions of interest (ROI) can be placed on any position in the B-mode output of an ultrasound scanner for acoustic intensity quantification.

After a peripheral intravenous injection of a small bolus of contrast, a trans-thoracic ultrasound transducer is positioned and fixed to show a four-chamber view (see Fig. 2). Therefore, the contrast can be detected for acoustic intensity curve measurements in both atria and ventricles. The acoustic intensity is determined as the average intensity in

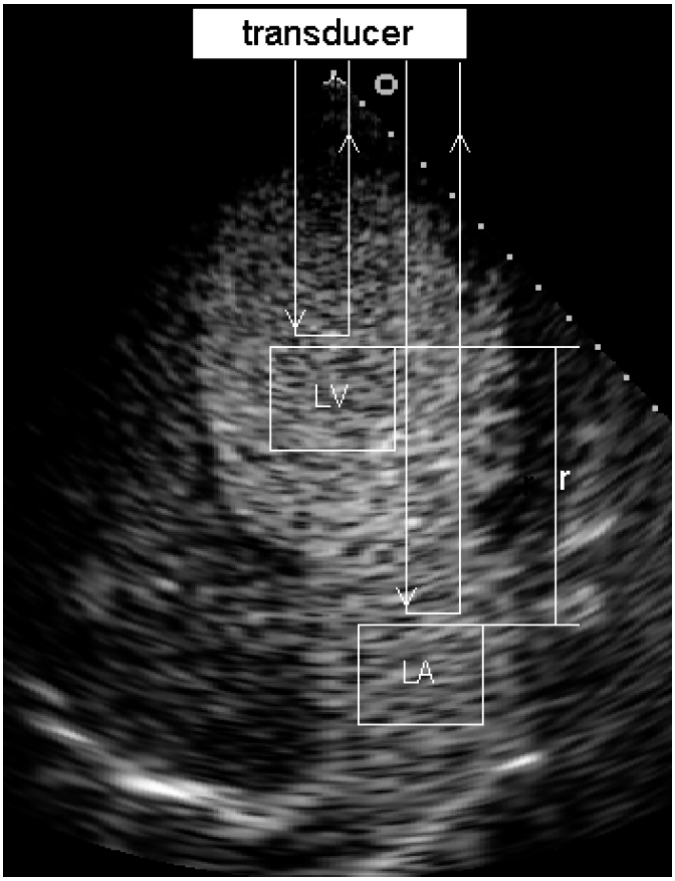

Fig. 2. Transthoracic, four-chamber view. Two ROIs are placed on the LV and LA for the IDC measurement. A simplified representation of the ultrasound wave paths to the LV and LA ROI are shown as well as the different distance r from the transducer.

the defined ROI. After the LA and LV acoustic intensity curves are measured (see Fig. 2 and Fig. 3), a deconvolution technique could estimate the impulse response of the system between the two sites (LV dilution system identification). However, a strict requirement is the linearity of the system. Although the contrast dilution system is linear, the relation between measured acoustic intensity and real contrast concentration is distorted by several nonlinearities.

In order to ensure a linear relation between contrast concentration and acoustic backscatter, the injected dose of contrast is very small (0.5 mg of SonoVue®, Bracco, Milan, Italy) [19]. In fact, the integrated acoustic backscatter is linearly related to contrast concentration in the low-concentration range [22], [32], [33], [36]. However, also according to experimental measurements, an attenuation effect is recognizable between LV and LA intensity curves [22], [32], [33], [36]. While the LV ROI is near the transducer, the LA ROI is beyond the LV and is detected by ultrasonic waves that pass twice through the contrast-filled LV (see Fig. 2). Consequently, as shown in Fig. 3, the LA acoustic backscatter is attenuated, and the LA intensity curve is lower than the LV curve.

The attenuation effect on the LV acoustic intensity curve is approximately constant (invariant with time), as it

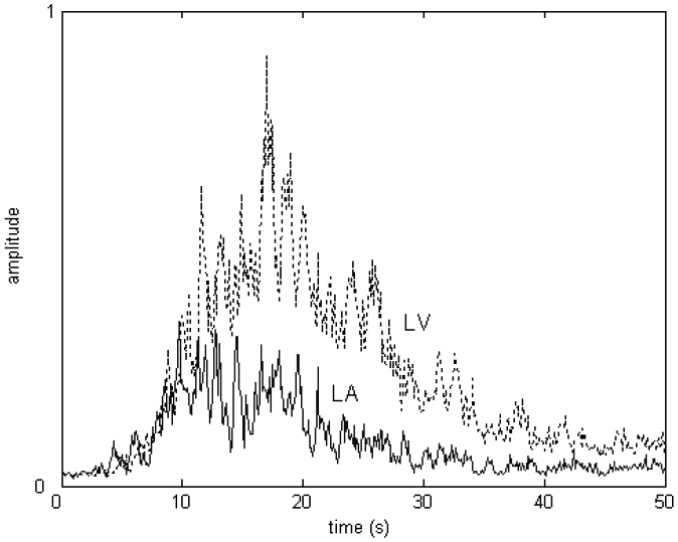

Fig. 3. LA and LV acoustic intensity curves. The LA curve shows a lower intensity due to the LV attenuation effect.

is mainly due to the tissue between the transthoracic transducer and the LV apex. Such an effect does not influence the linearity of the relation between contrast concentration and acoustic intensity. Nonlinearities are introduced by the attenuation between LV and LA ROI. As a consequence, the attenuation of the LV acoustic intensity is neglected, and the attenuation effect on the LA intensity curve can be compensated by exploiting the information derived from the LV acoustic intensity curve.

The acoustic intensity decay between LV and LA due to attenuation is described by an exponential relation as given in (6) [43], where $\widehat{I}_{LA}$ and I_{LA} represent the LA acoustic intensity with and without attenuation, a_t is the total attenuation coefficient, and r is the distance between the LA and LV ROI:

$$\widehat{I}_{LA} = I_{LA} \cdot e^{-2a_t r}. \tag{6}$$

The attenuation coefficient a_t is the sum of two terms ($a_t = a_1 + a_2$): the stationary attenuation coefficient a_1 due to physiological structures (tissue and blood) and the nonstationary attenuation coefficient a_2 due to diluted contrast. The standard value for a_1, which is used to estimate derated pressure values in tissue, is equal to 0.3 dB/cmMHz [44]. For small contrast concentrations, the attenuation coefficient is linearly related to the contrast concentration [26], [32], [36]. Therefore, the attenuation coefficient a_2 is linearly related to the contrast concentration in the LV C_{LV} ($a_2 = k_1 C_{LV}$). Due to the constant attenuation of the LV acoustic intensity I_{LV}, the relation between C_{LV} and I_{LV} is linear ($C_{LV} = k_2 I_{LV}$), and a_2 can be represented as a linear function of I_{LV}. With $k = 2k_1k_2r$, (6) is given as in (7).

$$\widehat{I}_{LA}(t) = I_{LA}(t) \cdot e^{-(2a_1 r + kI_{LV}(t))}. \tag{7}$$

Because a_1 and r are known, (7) contains only three unknowns, which are the constant coefficient k and the

nonattenuated intensities I_{LA} and I_{LV}. In order to estimate I_{LA}, two conditions have to be added. The first condition concerns the ratio b between the peak concentration in the LV and LA. This condition also can be expressed as $I_{LV_{\max}} = bI_{LA_{\max}}$, where $I_{LA_{\max}}$ and $I_{LV_{\max}}$ represent the maxima of the LA and LV intensity curves without attenuation. The second condition is derived from the assumption of neglectable attenuation of the LV acoustic intensity and is expressed as $I_{LV} = \widehat{I}_{LV}$. Combining these two conditions with (7), I_{LA} is derived from the measured (attenuated) intensities $\widehat{I}_{LA}$ and $\widehat{I}_{LV}$ as given in (8):

$$I_{LA}(t) = \widehat{I}_{LA}(t)e^{2a_1 r} \cdot \left(\frac{\widehat{I}_{LV_{\max}} e^{-2a_1 r}}{b\widehat{I}_{LA_{\max}}} \right)^{\left(\frac{\widehat{I}_{LV}(t)}{\widehat{I}_{LV_{\max}}} \right)}. \tag{8}$$

The distance r usually is fixed to 5 cm, and the ultrasound frequency is 1.9 MHz. As a result, $a_1 r = 0.328$. The ratio between peak concentrations in the LV and LA is difficult to determine. However, the final FEF measurements show reliable results when an equal peak concentration is considered. Therefore, the peak concentration ratio b is fixed to 1. Further research will include a specific experimentation for an accurate assessment of the concentration ratio b and its dependency on physiological parameters.

Eq. (8) expresses the LA acoustic intensity curve without attenuation I_{LA} as a function of attenuated measurements; therefore, it allows compensating for the attenuation effect on the measured LA intensity curve $\widehat{I}_{LA}$. After compensation, both the LA and LV intensity curves are linearly related to the contrast concentration; therefore, they are referred to as IDCs. The resulting IDCs are ready to be processed for the LV impulse response estimation.

C. LV Impulse Response Estimation

The fluid-dynamic dilution system between contrast injection and detection is a linear system. In fact, if two boluses of mass equal to αM and βM are injected ($\alpha, \beta \in \mathsf{R}$), the detected IDC, as from all the IDC models [18], [19], [21], [34], [35], equals $\alpha C(t) + \beta C(t)$. Therefore, once the LA and LV ultrasound intensity curves are transformed into IDCs by compensating for all the nonlinear effects, they can be used as inputs of a deconvolution algorithm for the estimation of the LV dilution-system impulse response [39].

In general, if $f(t)$ and $g(t)$ are the input and output functions of a linear system (e.g., the LA and LV IDCs for the LV system), $g(t)$ is the result of a convolution operation between the input $f(t)$ and the system impulse response $h(t)$ ($g(t) = h(t) * f(t)$). The impulse response $h(t)$ characterizes the linear system. In fact, if $f(t)$ is an impulse (Dirac function), $h(t) = g(t)$. However, when $f(t)$ is not an impulse, $h(t)$ still can be recovered from $f(t)$ and $g(t)$ by a deconvolution operation.

The UCA IDC measurements are influenced by several noise sources, such as bad mixing of the contrast, acoustic reverberation, backscatter oscillations due to pressure variations, bubble disruption due to ultrasound pressure, patient movement and blood-acceleration artifacts, and contrast recirculation, resulting in very noisy IDCs. Due to the small SNR, direct deconvolution techniques based on either matrix inversion in time domain or spectrum inversion in frequency domain fail [39]. In fact, although these direct deconvolution techniques are rather simple, difficulties arise as soon as the SNR decreases.

The signal to be deconvoluted, i.e., the LV IDC, is given as $G(\omega) = F(\omega)H(\omega) + N(\omega)$, where $F(\omega)$ is the LA IDC, $H(\omega)$ is the LV impulse response, and $N(\omega)$ is the noise frequency spectrum. The result of a direct deconvolution in frequency domain, i.e., the input response estimate $\widehat{H}(\omega)$, is given as in (9).

$$\widehat{H}(\omega) = \frac{G(\omega)}{F(\omega)} = H(\omega) + \frac{N(\omega)}{F(\omega)}. \tag{9}$$

The division of the noise spectrum $N(\omega)$ by $F(\omega)$ generates a high-frequency noise amplification because the noise band usually is larger than the signal $F(\omega)$ band. Especially for IDC applications, $F(\omega)$ contains only low-frequency components and $N(\omega)$ is a broad-band noise. As a consequence, the high-pass filter $F^{-1}(\omega)$ works as a noise amplifier, and the deconvolution operation becomes very unstable.

A possible solution is the use of a least square technique, such as a Wiener deconvolution filtering [39]–[42], [45]. It is a least square estimation of the optimum deconvolution filter $w(t)$. This method aims to minimize the L^2 distance $d(g(t) * w(t), h(t))$, which is defined as $d(w) = \int (g(t) * w(t) - h(t))^2 dt$.

The minimum distance is given by the zero crossing of the derivative of d with respect to w. It is solution of the equation $d'(w) = 0$, which can be expressed as given in (10), where R_{hg} and R_{gg} represent the correlation between $h(t)$ and $g(t)$ and the autocorrelation of $g(t)$, respectively.

$$R_{hg}(t) = w(t) * R_{gg}(t). \tag{10}$$

Eq. (10) is referred to as normal Wiener-Hopf equation. For uncorrelated noise, $R_{hg}(t) = R_{hn}(t) + R_{hh}(t) * f(-t) = R_{hh}(t) * f(-t)$ and $R_{gg}(t) = 2R_{hn}(t) * f(-t) + R_{ff}(t) * R_{hh}(t) + R_{nn}(t) = R_{ff}(t) * R_{hh}(t) + R_{nn}(t)$. Therefore, in frequency domain, $W(\omega)$ is given as in (11), where $S_{ff}(\omega)$, $S_{hh}(\omega)$, and $S_{nn}(\omega)$ are the LA IDC input function, the LV impulse response, and the noise power spectrum respectively.

$$W(\omega) = \frac{F^*(\omega)}{S_{ff}(\omega) + \frac{S_{nn}(\omega)}{S_{hh}(\omega)}}. \tag{11}$$

Eq. (11) corresponds to a direct deconvolution filter in frequency domain except for the term $S_{nn}(\omega)/S_{hh}(\omega)$, which corresponds to the SNR spectrum. It represents the typical design of a Wiener deconvolution filter, whose bidimensional version was already applied to B-mode echography in order to compensate for the point spread func-

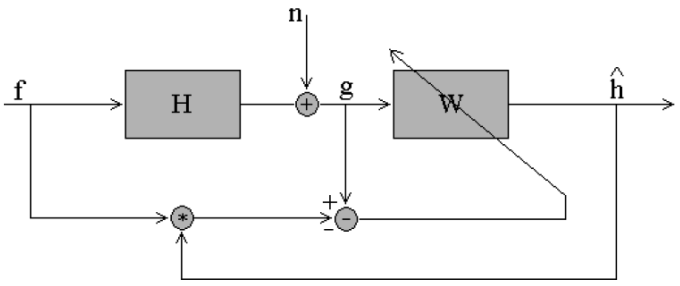

Fig. 4. Scheme of the implemented adaptive Wiener deconvolution algorithm.

tion and increase the scanner resolution [46]–[48]. However, such an application required the estimate of both the impulse response function $h(t)$ and the input function $f(t)$, which represented the ultrasound pulse, resulting in a blind deconvolution. The increased complexity of the problem was solved by using a homomorphic deconvolution approach, i.e., mapping the space domain into the complex logarithmic Fourier domain (referred to as cepstrum) [49], [50]. In the presented application the input function $f(t)$ is measured, and the standard Wiener deconvolution filter is adopted.

The LV impulse response power spectrum $S_{hh}(\omega)$ can be derived from the exponential model in (3) and expressed as $C_0^2\tau^2/(1+\tau^2\omega^2)$. Due to the broad-band characteristic, the noise power spectrum $S_{nn}(\omega)$ can be approximated by a constant N^2 (white noise) [18]. As a result, (11) can be expressed as given in (12):

$$W(\omega) = \frac{F^*(\omega)}{S_{ff}(\omega) + (N^2/C_0^2\tau^2)(1+\tau^2\omega^2)}. \tag{12}$$

An adaptive version of the filter is realized as shown in Fig. 4 [51]. An iterative process minimizes the L^2 distance $d(g(t),\ f(t) * \widehat{h}(t))$ by changing the parameters τ^2 and $N^2C_0^2$ of the Wiener filter in (12). Because the designed Wiener filter is implemented in Matlab® (The MathWorks, Natick, MA), the adopted minimization algorithm is the Nelder-Mead Simplex Method that is available in the Matlab® optimization toolbox [52].

Especially for low SNR, the algorithm shows long convergence time. Therefore, a suboptimal design of the Wiener filter is considered. The SNR is assumed to be constant [41], [47], so that iterations only involve the optimization of one parameter. In addition, a finite impulse response (FIR) low-pass prefilter made of 5 taps (about 1/4 of the cardiac cycle for sampling frequency equal to 20 Hz) is applied to both $g(t)$ and $f(t)$ in order to reduce the high-frequency noise components before deconvolution. Several prefilters have been tested; however, larger prefilters do not lead to further improvements.

The adaptive Wiener filter is applied to the measured LV IDC to estimate the LV impulse response, which is fitted by the exponential monocompartment model as shown in Fig. 5 and interpreted by (5) for the FEF estimate. In fact, the LV impulse response that is estimated after the attenuation compensation in (7) and the deconvolution filter in Fig. 4 fulfills the requirements for the application of (5). The exponential model is fitted to the impulse response down-slope by a multivariate linear regression in the logarithmic domain. It is fitted between 80% and 10% of the impulse response peak amplitude (see Fig. 5).

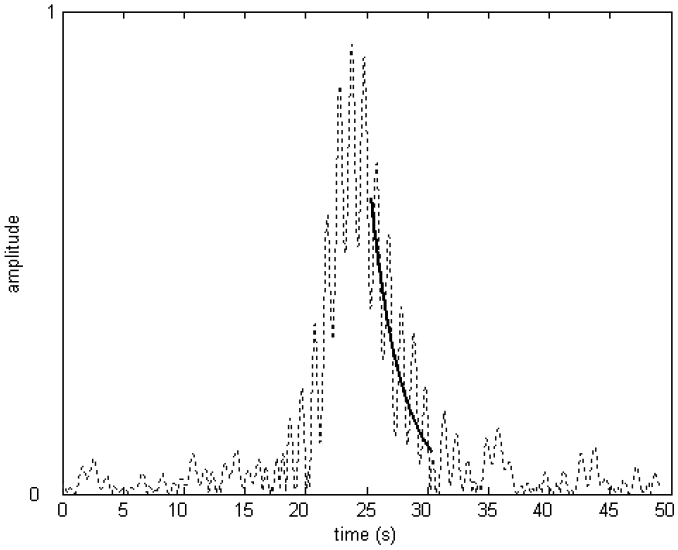

Fig. 5. LV impulse response (dashed line) derived by Wiener deconvolution of a real signal. The exponential model (solid line) fits the curve along the down-slope between 80% and 10% of the peak amplitude.

The final design of the deconvolution filter was tested by specific simulations. Classic L^2 SNR definitions would depend on signal length, since the SNR is non-stationarity. Therefore, the SNR was defined as $20\log(A_{\max}/N)$, where $A_{\max}$ is the peak amplitude of the signal (IDC) and N is the noise amplitude. The input IDC $f(t)$ was generated according to the local density random walk (LDRW) model, which was introduced by Sheppard and Savage in 1951 [53]. The model is solution of the diffusion equation [35] and shows the best least square estimation of the IDC [18], [54]–[58]. White noise was added for SNR equal to 10 dB, 15 dB, 20 dB, and ∞. No measured IDC shows an SNR smaller than 15 dB (see Fig. 6). The $f(t)$ was then convoluted with a monocompartment impulse response (exponential decay $h(t)$) to obtain the output IDC $g(t)$. White noise was also added to $g(t)$, and the same SNRs as for $f(t)$ were generated.

The monocompartment impulse response was varied in order to generate FEFs going from 10% to 80%, which cover the real application range. Figs. 7 and 8 show the simulation results in terms of average values and standard deviations over 1000 different noise sequences for each SNR and FEF.

The algorithm shows robustness even in the case of very low SNR. The correlation coefficients are 0.9964, 0.9993, 0.9999, and 1 for SNR going from 10 dB to ∞. However, when the FEF increases, an average underestimation is recognizable for low SNR.

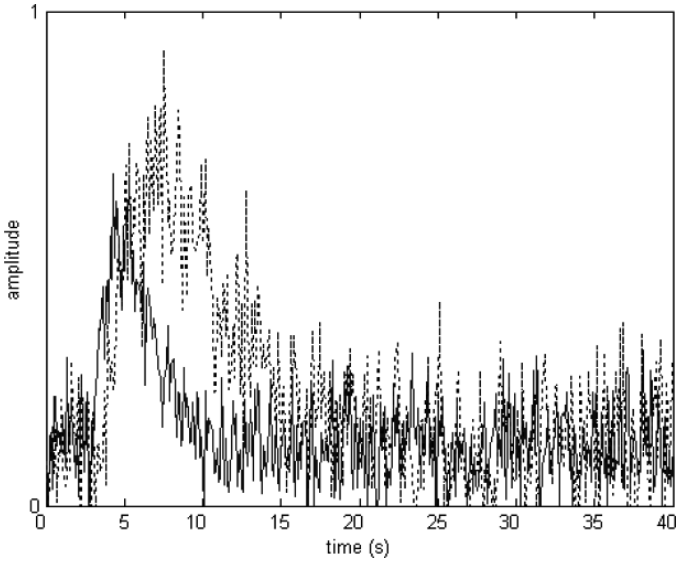

Fig. 6. Example of simulated IDCs for SNR = 15 dB.

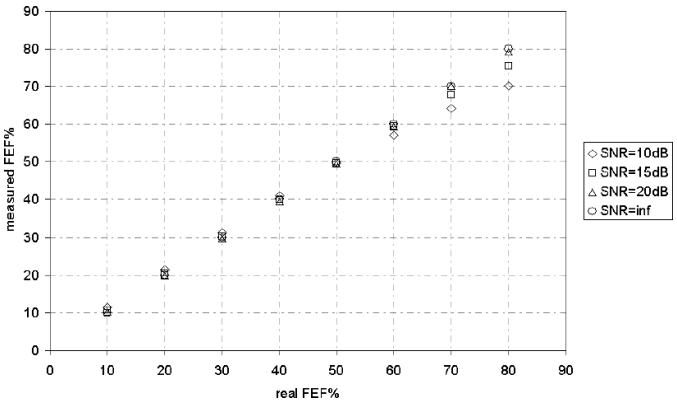

Fig. 7. Simulation results. EF average estimates for different SNR and EF over 1000 different noise sequences.

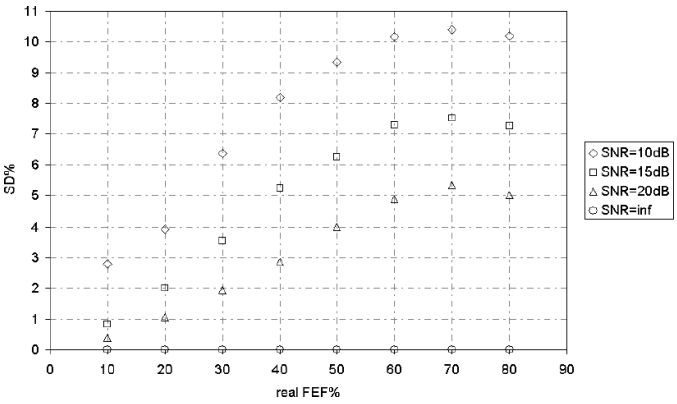

Fig. 8. Simulation results. Standard deviation (SD) for different SNR and EF over 1000 different noise sequences.

D. Validation Setup

The use of the Wiener deconvolution approach to estimate impulse-response functions of UCA dilution systems was preliminary tested in vitro. The setup described in [19] was adopted. Two IDCs were measured at the inflow and outflow of a predetermined volume, and the dilution impulse response was estimated. The estimated impulse response then was fitted by the LDRW model for the volume assessment. The results showed a determination coefficient of the volume measurements equal to 0.99 and a standard deviation smaller than 3.1% for flow ranging from 1 to 5 L/minute [59].

These results proved the accuracy and feasibility of the impulse-response Wiener estimation, and the system then was tested for the FEF assessment in patients, which is the main objective of this paper. A 10 ml bolus of SonoVue® contrast agent diluted 1:100 into saline (0.9% NaCl) was injected intravenously and detected in B-mode by an ultrasound scanner Sonos 5500 (Philips Medical Systems, Andover, MA). A transthoracic S3 probe was positioned to show a four-chamber view. Software Q-Lab® (Philips Medical Systems) for acoustic quantification was used to measure the acoustic intensity curves. Two ROI were placed on the LA and LV for the acoustic intensity curve measurements.

The scanner was set in power modulation mode in order to enhance the signal backscattered by the contrast. Series of three adjacent ultrasound pulses of four cycles at 1.9 MHz were transmitted. The amplitude of the central pulse is twice that of the side pulses. The receiver sums the reflections of the side pulses and subtracts the reflection of the central pulse. This technique, which is a specific implementation of the power modulation mode, allows detecting the nonlinear response of bubbles while cancelling the linear response of tissue. The result is an increased sensitivity of the scanner to the contrast bubbles diluted in both the LA and the LV. A low mechanical index (i.e., the ratio between peak rarefactional pressure expressed in megapascal and square root of the central frequency of the ultrasound pulse expressed in megahertz) equal to 0.1 allowed minimizing bubble destruction. For low contrast concentrations, this harmonic imaging setting shows a very high correlation coefficient between contrast concentration and backscattered acoustic power [19].

The contrast agent SonoVue® is composed of microbubbles enclosed in a monolayer phospholipid shell. The inner gas is SF_6 (sulphur hexafluoride). It is a large molecule that does not diffuse easily through the shell, resulting in a high stability of the bubbles. The bubble diameter is distributed from 0.7 μm to 10 μm with a mean value equal to 2.5 μm [28], [60].

The measured acoustic intensity curves were transformed into IDCs by attenuation compensation and analyzed off-line for the FEF assessment. The analysis was implemented on a computer using both LabView® (National Instruments, Austin, TX) and Matlab® (The MathWorks, Natick, MA) software.

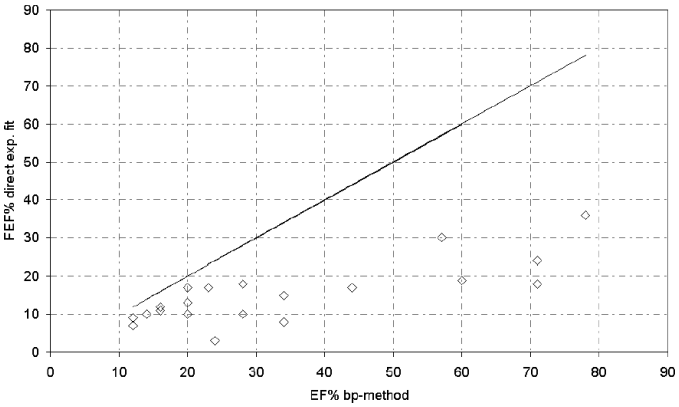

Fig. 9. FEF measurements without use of deconvolution. The FEF is directly measured from the LV IDC exponential fit. The results show an evident underestimation with respect to EF echocardiographic bi-plane estimates.

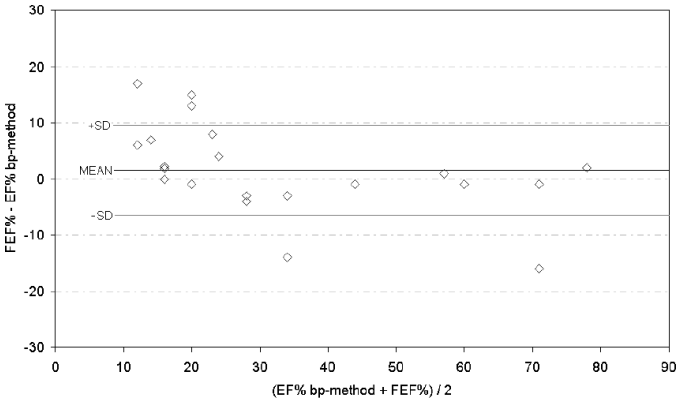

Fig. 10. Bland-Altman plot of the EF and FEF estimates by dilution and bi-plane echographic methods.

A group of 20 patients with EF going from 10% to 70% and no significant mitral insufficiency ($EF \simeq FEF$) was selected (this study was approved by the Ethics Committee of the Catharina Hospital, Eindhoven, The Netherlands). The FEF estimates were compared to EF measurements obtained by echographic bi-plane method on two- and four-chamber views with contrast opacification. The average over three EF measurements was considered as the reference value to validate the FEF estimates.

III. Results

The results of a preliminary study on 20 patients are presented. The FEF estimates are compared to the echographic bi-plane method with contrast opacification. Fig. 9 shows the FEF estimates using the exponential fit of the measured LV IDC without deconvolution. As expected, there is a large FEF underestimation. In fact, the contrast bolus is injected in an arm vein, and the hypothesis of fast injection in the LV for the application of (5) is not fulfilled.

Instead, the use of the proposed deconvolution approach results in a correlation coefficient equal to 0.93 between the ejection fraction estimates made by the proposed method and the echographic bi-plane method. Fig. 10 shows the Bland-Altman plot for the two compared techniques [61]. The bias equals 1.6% and the standard deviation (SD) equals 8%. Taking into account that comparisons of different EF measurement techniques always show significant standard deviations (usually larger than 15% [4], [11]), these preliminary results are promising and prove the feasibility of the method. The FEF estimates are shown in Fig. 11 together with the bi-plane EF estimates.

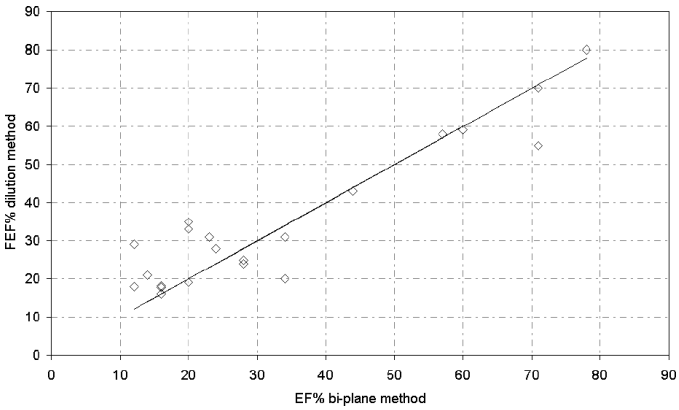

Fig. 11. FEF estimates compared to EF estimates by bi-plane echocardiographic method after contrast opacification.

IV. Conclusions

The LV EF is an important parameter for the assessment of the cardiac condition and efficiency. Accurate EF measurements require experienced cardiologists and time-consuming geometric imaging techniques. In clinical practice, bi-dimensional imaging methods are widely used. Because they make use of geometrical models, anatomical abnormalities (for instance an aneurysm) are not detected and taken into account for the EF estimation. Moreover, such geometric methods can assess only the total EF, without distinction between forward and backward EF, which is caused by mitral insufficiency.

The indicator dilution method is an alternative solution, which can be used for FEF measurements. However, both contrast injection and detection must be performed in the LV, resulting in very invasive techniques.

A new minimally invasive technique based on UCA dilution is presented. A small bolus of UCA is injected in a peripheral vein and detected in the LA and LV by a transthoracic ultrasound transducer. The detected acoustic intensity is processed in order to obtain the LA and LV IDCs. A deconvolution algorithm is implemented in order to estimate the impulse response of the LV. The resulting curve is analyzed for the LV FEF assessment.

The method was tested and optimized by specific simulations for different noise levels. Eventually, the feasibility of the measurement was tested in vivo. The EF was mea-

sured on a group of 20 patients both by the proposed dilution method and the echographic bi-plane method. This preliminary validation proves the feasibility of the dilution method and encourages further evaluations and optimization for in-vivo applications. The peak-concentration ratio between LV and LA will be determined by specific experimentation. Future research plans also include the comparison of the dilution method with MRI EF measurements, which may be considered as the gold standard.

Apart from the LV FEF measurement, this technique also opens new possibilities for the assessment of regurgitant EF, which is caused by mitral insufficiency. In fact, the difference between EF and FEF is due to blood regurgitation and could be quantified by comparing dilution and geometric estimates.

Other immediate applications could involve right ventricle FEF measurements. The right ventricle EF cannot be measured by geometric imaging techniques as the shape is difficult to model. The proposed method could allow measuring the right ventricle FEF and provide cardiologists with a new valuable diagnostic parameter. Further applications, involving for instance the measurement of intrathoracic blood volumes, also are being investigated.

Appendix A

Eq. (4) is the impulse response of a monocompartment model. A chamber of volume V with only one input and one output represents the compartment. A fluid flows through the chamber. If the chamber is not elastic and the fluid incompressible, the input and output flow Q are equal. If an indicator mass M is diluted in the chamber with concentration C, for the mass conservation principle it follows that $dM = dCV = VdC + CdV = 0$, i.e., the change of indicator mass in the chamber $VdC(t)$ equals the indicator mass $C(t)dV$ that leaves the chamber. Therefore, because $C(t)dV = C(t)Qdt$, the system can be described by a differential equation as given in (13):

$$VdC(t) = -C(t)Qdt. \tag{13}$$

Eq. (4) is the solution of (13) for initial concentration $C(0) = C_0$ and time constant $\tau = V/Q$.

References

[1] P. Brigger, P. Bacharach, A. Aldroubi, and M. Unser, "Segmentation of gated spect images for automatic computation of myocardial volume and ejection fraction," in *IEEE Proc. Int. Conf. Image Processing*, Oct. 1997, pp. 113–116.

[2] A. Khorsand, S. Graf, C. Pirich, G. Wagner, D. Moertl, H. Frank, K. Kletter, H. Sochor, G. Maurer, E. Schuster, and G. Porenta, "Image analysis of gated cardiac pet to assess left ventricular volumes and contractile function," in *IEEE Proc. Comput. Cardiol.*, Sep. 2000, pp. 311–314.

[3] R. J. van der Geest, E. Jansen, V. G. M. Buller, and J. H. C. Reiber, "Automated detection of left ventricular epi- and endocardial contours in short-axis mr images," in *IEEE Proc. Comput. Cardiol.*, Sep. 1994, pp. 33–36.

[4] S. Schalla, E. Nagel, H. Lehmkuhl, A. B. C. Klein, B. Schnackenburg, U. Schneider, and E. Fleck, "Comparison of magnetic resonance real-time imaging of left ventricular function with conventional magnetic resonance imaging and echocardiography," *Amer. J. Cardiol.*, vol. 87, pp. 95–99, 2001.

[5] W. C. Brogan, B. Glamann, and L. D. Hillis, "Comparison of single and biplane ventriculography for determination of left ventricular volume and ejection fraction," *Amer. J. Cardiol.*, vol. 69, no. 12, pp. 1079–1082, 1992.

[6] T. Shiota, P. M. McCarthy, R. D. White, J. X. Quin, N. L. Greenberg, S. D. Flamm, J. Wong, and J. D. Thomas, "Initial clinical experience of real-time three-dimensional echocardiography in patients with ischemic and idiopathic dialated cardiomyopathy," *Amer. J. Cardiol.*, vol. 84, pp. 1068–1073, 1999.

[7] W. A. Helbing, H. G. Bosch, C. Maliepaard, S. A. Rebergen, R. J. van der Geest, B. Hansen, J. Ottenkamp, J. H. C. Reiber, and A. de Roos, "Comparison of echocardiographic methods with magnetic resonance imaging for assessment of right ventricular function in children," *Amer. J. Cardiol.*, vol. 76, pp. 589–594, 1995.

[8] H. Feigenbaum, *Echocardiography*. Philadelphia, PA: Lippincott Williams & Wilkins, 1994.

[9] L. E. Teichholz, T. Kreulen, M. V. Herman, and R. Gorlin, "Problems in echocardiographic volume determinations: Echocardiographic-angiographic correlations in the presence or absence of asynergy," *Yale J. Biol. Med.*, vol. 66, pp. 397–413, 1994.

[10] G. de Simone, R. B. Devereux, A. Ganau, R. T. Hahn, P. S. Saba, G. F. Mureddu, M. J. Roman, and B. V. Howard, "Estimation of left ventricular chamber and stroke volume by limited M-mode echocardiography and validation by two-dimensional and doppler echocardiography," *Amer. J. Cardiol.*, vol. 78, pp. 801–807, 1996.

[11] N. G. Bellenger, M. I. Burgess, S. G. Ray, A. Lahiri, A. J. Coats, J. G. Cleland, and D. J. Pennell, "Comparison of left ventricular ejection fraction and volumes in heart failure by echocardiography, radionuclides, ventriculography and cardiovascular magnetic resonance. Are they interchangeable?," *Eur. Heart*, vol. 21, no. 16, pp. 1387–1396, 2000.

[12] J. D. Bronzino, Ed. *The Biomedical Engineering Handbook*. 2nd ed. Boca Raton, FL: CRC Press, 2000.

[13] N. Gefen, O. Barnea, A. Abramovich, and W. P. Santamore, "Experimental assessment of error sources in thermodilution measurements of cardiac output and ejection fraction," in *IEEE Proc. First Joint Biomed. Eng. Soc./Eng. Med. Biol. Soc. Conf. Serving Humanity, Advancing Technology*, 1999, p. 796.

[14] J. P. Holt, "Estimation of residual volume of the ventricle of the dog by two indicator dilution techniques," *Circ. Res.*, vol. 4, no. 2, pp. 187–195, Mar. 1956.

[15] S. Jang, R. J. Jaszczak, J. Li, J. F. Debatin, S. N. Nadel, A. J. Evans, K. L. Greer, and R. E. Coleman, "Cardiac ejection fraction and volume measurements using dynamic cardiac phantoms and radionuclide imaging," *IEEE Trans. Nuclear Sci.*, vol. 41, no. 6, pp. 2845–2849, 1994.

[16] T. Machnig, B. Eicker, K. Barth, H. Lehmkuhl, and K. Bachmann, "Measurement of left ventricular ejection fraction (ef) by densitometry from digital subtraction angiography," in *IEEE Proc. Comput. Cardiol.*, Sep. 1990, pp. 589–592.

[17] H. Becher and P. N. Burns, *Handbook of Contrast Echography*. New York: Springer-Verlag, 2000.

[18] M. Mischi, A. A. C. M. Kalker, and H. H. M. Korsten, "Videodensitometric methods for cardiac output measurements," *Eurasip J. Appl. Signal Processing*, vol. 2003, no. 5, pp. 479–489, 2003.

[19] M. Mischi, A. A. C. M. Kalker, and H. H. M. Korsten, "Contrast echocardiography for pulmonary blood volume quantification," *IEEE Trans. Ultrason., Ferroelect., Freq. Contr.*, vol. 51, no. 9, pp. 1137–1147, Sep. 2004.

[20] M. Mischi, A. A. C. M. Kalker, and H. H. M. Korsten, "Blood volume measurements by videodensitometric analysis of ultrasound-contrast-agent dilution curves," in *Proc. Int. Conf. IEEE Eng. Med. Biol. Soc.*, Sep. 2003, pp. 791–794.

[21] X. Chen, K. Q. Schwarz, D. Phillips, S. D. Steinmetz, and R. Schlief, "A mathematical model for the assessment of hermodynamic parameters using quantitative contrast echocardiography," *IEEE Trans. Biomed. Eng.*, vol. 45, no. 6, pp. 754–765, 1998.

[22] C. S. Sengel and P. H. Arger, "Mathematical modeling of dilution curves for ultrasonographic contrast," *J. Ultrasound Med.*, vol. 16, pp. 471–479, 1997.

[23] P. A. Heidenreich, J. G. Wiencek, J. G. Zaroff, S. Aroson, L. J. Segil, P. V. Haper, and S. B. Feinstein, "In vitro calculation of flow by use of contrast ultrasonography," *J. Amer. Soc. Echocardiogr.*, vol. 6, no. 1, pp. 51–61, 1993.

[24] D. Rovani, S. E. Nissen, E. Jonathan, M. Smith, A. L'Abbate, O. L. Kuan, and A. N. DeMaria, "Contrast echo washout curves from left ventricle: Application of basic principles of indicator-dilution theory and calculation of ejection fraction," *J. Amer. Coll. Cardiol.*, vol. 10, pp. 125–134, 1987.

[25] K. Mizushige, A. N. DeMaria, Y. Toyama, H. Morita, S. Senda, and H. Matsuo, "Contrast echocardiography for evaluation of left ventricular flow dynamics using densitometric analysis," *Circulation*, vol. 88, pp. 588–595, 1993.

[26] H. Bleeker, K. Shung, and J. Barnhart, "On the application of ultrasonic contrast agents for blood flowmetry and assessment of cardiac perfusion," *Ultrasound Med. Biol.*, vol. 9, pp. 461–471, 1990.

[27] L. Gerfault, E. Helms, V. Bailleau, N. Rognin, G. Finet, M. Janier, and C. Cachard, "Assessing blood flow in isolated pig heart with usca," in *Proc. IEEE Ultrason. Symp.*, Oct. 1999, pp. 1725–1728.

[28] J. M. Gorce, M. Arditi, and M. Schneider, "Bubble oscillations of large amplitude," *Invest. Radiol.*, vol. 35, no. 11, pp. 661–671, 2000.

[29] M. Postema, A. Bouakaz, and C. T. Chin, "Simulations and measurements of optical images of insonified ultrasound contrast microbubbles," *IEEE Trans. Ultrason., Ferroelect., Freq. Contr.*, vol. 50, pp. 523–536, 2003.

[30] L. Hoff, *Acoustic Characterization of Contrast Agents for Medical Ultrasound Imaging*. Dordrecht, The Netherlands: Kluwer Academica, 2001.

[31] P. J. A. Frinking and N. de Jong, "Acoustic modeling of shell encapsulated gas bubbles," *Ultrasound Med. Biol.*, vol. 24, no. 4, pp. 523–533, 1998.

[32] A. Bouakaz, N. de Jong, and C. Cachard, "Standard properties of ultrasound contrast agents," *Ultrasound Med. Biol.*, vol. 24, no. 3, pp. 469–472, 1996.

[33] V. Uhlendorf, "Physics of ultrasound contrast imaging: Scattering in the linear range," *IEEE Trans. Ultrason., Ferroelect., Freq. Contr.*, vol. 41, no. 1, pp. 70–79, 1994.

[34] C. W. Sheppard, *Basic Principles of Tracer Methods: Introduction to Mathematical Tracer Kinetics*. New York: Wiley, 1962.

[35] K. H. Norwich, *Molecular Dynamics in Biosystems*. New York: Pergamon, 1977.

[36] B. Herman, S. Einav, and Z. Vered, "Feasibility of mitral flow assessment by echo-contrast ultrasound. Part I: Determination of the properties of echo-contrast agents," *Ultrasound Med. Biol.*, vol. 26, no. 5, pp. 785–795, 2000.

[37] W. R. Hedrick, D. L. Hykes, and D. E. Starchman, *Ultrasound Physics and Instrumentation*. 3rd ed. Naples, Italy: Mosby, 1995.

[38] N. de Jong, A. Bouakaz, and F. J. T. Cate, "Contrast harmonic imaging," *Ultrasonics*, vol. 40, no. 1, pp. 567–573, 2002.

[39] P. A. Jansson, *Deconvolution of Images and Spectra*. New York: Academic, 1997.

[40] A. Papoulis, *Probability, Random Variables, and Stochastic Processes*. 3rd ed. New York: McGraw-Hill, 1991.

[41] A. M. Guarnieri, F. Rocca, P. Guccione, and C. Cafforio, "Optimal interferometric scansar focusing," in *Proc. IEEE Geosci. Remote Sensing Symp.*, June 1999, pp. 1718–1720.

[42] Y. Jeong, H. Ryou, and C. Lee, "A high resolution delay estimation technique in frequency domain for positioning systems," in *Proc. IEEE Vehicular Technol. Conf.*, Sep. 2002, pp. 2318–2321.

[43] P. N. T. Wells, *Biomedical Ultrasonics*. New York: Academic, 1977.

[44] "Information for manufacturers seeking marketing and clearance of diagnostic ultrasound systems and transducers," U.S. Department of Health and Human Services, Food and Drug Administration, Center for Devices and Radiological Health, Tech. Rep. Sep. 30, 1997.

[45] A. P. Dhawan, *Medical Image Analysis*. Hoboken, NJ: Wiley, 2003.

[46] T. Taxt and J. Strand, "Two-dimensional noise-robust blind deconvolution of ultrasound images," *IEEE Trans. Ultrason., Ferroelect., Freq. Contr.*, vol. 48, no. 4, pp. 861–866, 2001.

[47] T. Taxt and G. V. Frolova, "Noise robust one-dimensional blind deconvolution of medical ultrasound images," *IEEE Trans. Ultrason., Ferroelect., Freq. Contr.*, vol. 46, no. 2, pp. 291–299, 1999.

[48] T. Taxt, "Restoration of medical ultrasound images using two-dimensional homomorphic deconvolution," *IEEE Trans. Ultrason., Ferroelect., Freq. Contr.*, vol. 42, no. 4, pp. 543–554, 1995.

[49] O. G. Jensen and P. P. Papazis, "Homomorphic deconvolution of potential field data in one or two dimensions," *Can. J. Earth. Sci.*, vol. 20, pp. 1260–1281, 1983.

[50] J. A. Jensen, "Deconvolution of ultrasound images," *Ultrason. Imag.*, vol. 14, no. 1, pp. 1–15, 1992.

[51] I. Y. Soon and S. N. Koh, "Speech enhancement using 2-d Fourier transform," *IEEE Trans. Speech Audio Processing*, vol. 11, no. 6, pp. 717–724, 2003.

[52] J. C. Lagarias, J. A. Reeds, M. H. Wright, and P. E. Wright, "Convergence properties of the Nelder-Mead simplex method in low dimensions," *SIAM J. Optim.*, vol. 9, no. 1, pp. 112–147, 1998.

[53] C. W. Sheppard and L. J. Savage, "The random walk problem in relation to the physiology of circulatory mixing," *Phys. Rev.*, vol. 83, pp. 489–490, 1951.

[54] J. M. Bogaard, J. R. C. Jansen, E. A. von Reth, A. Versprille, and M. E. Wise, "Random walk type models for indicator-dilution studies: Comparison of a local density random walk and a first passage times distribution," *Cardiovasc. Res.*, vol. 20, no. 11, pp. 789–796, 1986.

[55] E. A. von Reth and J. M. Bogaard, "Comparison of a two-compartment model and distributed models for indicator dilution studies," *Med. Biol. Eng. Comput.*, vol. 21, pp. 453–459, 1983.

[56] J. M. Bogaard, S. J. Smith, A. Versprille, M. E. Wise, and F. Hagemeijer, "Physiological interpretation of skewness of indicator-dilution curves: Theoretical considerations and practical application," *Basic Res. Cardiol.*, vol. 79, pp. 479–493, 1984.

[57] M. E. Wise, "Tracer dilution curves in cardiology and random walk and lognormal distributions," *Acta Physiol. Pharmacol. Neerl.*, vol. 14, pp. 175–204, 1966.

[58] R. K. Millard, "Indicator-dilution dispersion models and cardiac output computing methods," *Amer. Physiol. Soc.*, vol. 272, no. 4, pp. H2004–H2012, 1997.

[59] M. Mischi, A. A. C. M. Kalker, and H. H. M. Korsten, "Identification of ultrasound-contrast-agent dilution systems for cardiac quantification," in *Proc. IEEE Int. Joined Symp.*, Aug. 2004.

[60] M. Shneider, "Influence of bubble size distribution on echogenecity of ultrasound contrast agents: A study of sonovue," *Echocardiography*, vol. 16, no. 7, pp. 743–746, 1999.

[61] J. M. Bland and D. G. Altman, "Statistical methods for assessing agreement between two methods of clinical measurement," *Lancet*, vol. 1, pp. 307–310, 1986.

Massimo Mischi was born in Rome, Italy, in 1973. In 1999 he received his M.S. degree in electronic engineering at La Sapienza University of Rome. In his final thesis he designed and validated a new device for optical-performance measurements of clinical fiber-optic endoscopes. In 2002 he completed a 2-year post-master program in technological design, information and communication technology, at the Eindhoven University of Technology, Eindhoven, The Netherlands, studying on the application of indicator dilution theory and ultrasound contrast agents for cardiac output measurements. Currently he is a Ph.D. candidate and a research assistant at the Eindhoven University of Technology.

His research concerns the quantification of cardiac parameters by means of contrast echocardiography. He is a student member of IEEE. He also is registered in the Italian Public Register of Engineers and in the Dutch Royal Institute of Engineers.

Annemieke Jansen was born in the Netherlands in 1965. She studied medicine at the University of Maastricht in the Netherlands. She was trained as a cardiologist in the Catharina Hospital in Eindhoven in the Netherlands, where she is currently finishing her Ph.D. study on the field of echocardiography for predicting the response to cardiac resynchronization therapy.

Antonius Kalker was born in The Netherlands in 1956. He received his M.S. degree in mathematics in 1979 from the University of Leiden, The Netherlands. From 1979 until 1983, while he was a Ph.D. candidate, he worked as a research assistant at the University of Leiden. From 1983 until December 1985 he worked as a lecturer at the Computer Science Department of the Technical University of Delft, Delft, The Netherlands. In January 1986 he received his Ph.D. degree in Mathematics.

In December 1985 he joined the Philips Research Laboratories Eindhoven, Eindhoven, The Netherlands. Until January 1990 he worked in the field of computer aided design. He specialized in (semi-) automatic tools for system verification. Currently he is a member of the Digital Signal Processing group of Philips Research. His research interests include wavelets, multirate signal processing, motion estimation, psycho-physics, digital video compression, medical imaging, digital watermarking and multimedia security. He is a Fellow of the IEEE.

Hendrikus Korsten was born in The Netherlands in 1953. He studied medicine in the University of Gronigen, Groningen, The Netherlands, and graduated as a medical doctor in 1978. During his training as an anesthesiologist in the St. Antonius Hospital in Utrecht, The Netherlands, he started his study for a Ph.D. degree on the measurement of intrathoracic fluid content during open-heart surgery. In November 1984 he received his Ph.D. degree in Medicine from the University of Leiden, The Netherlands.

Since June 1982 until now, he has been a staff-member of the Department of Anesthesiology, Intensive Care and Pain Treatments in the Catharina Hospital, Eindhoven, The Netherlands. From 1989 until 1993 he was the chairman of the professional medical staff of this hospital (a large teaching hospital in the south of The Netherlands). He is also an Intensivist and was head of the Intensive Care during the period 1993 until 2001. During this period he was one of the initiators of a national intensive-care database. He was also involved in research projects on data storage and data mining of patient data, as well as the development of artificial intelligence in the intensive-care. In 2001 he was appointed professor at the Department of Electrical Engineering, Eindhoven University of Technology, The Netherlands.